



Contents lists available at ScienceDirect

Spectrochimica Acta Part A: Molecular and Biomolecular Spectroscopy

journal homepage: www.elsevier.com/locate/saa

Thermal, spectroscopic, electrochemical, and electroluminescent characterization of malononitrile derivatives with triphenylamine structure

Danuta Sęk^a, Sonia Kotowicz^b, Sławomir Kula^b, Mariola Siwy^a, Agata Szłapa-Kula^b, Jan Grzegorz Małecki^b, Sebastian Maćkowski^c, Ewa Schab-Balcerzak^{a,b,*}

^a Centre of Polymer and Carbon Materials, Polish Academy of Sciences, 34 M. Curie-Skłodowska Str., 41-819 Zabrze, Poland

^b Institute of Chemistry, University of Silesia, 9 Szkolna Str., 40-006 Katowice, Poland

^c Institute of Physics, Faculty of Physics, Astronomy and Informatics, Nicolaus Copernicus University, 5 Grudziadzka Str., 87-100 Torun, Poland

ARTICLE INFO

Article history:

Received 2 August 2018

Received in revised form 2 October 2018

Accepted 12 November 2018

Available online 13 November 2018

Keywords:

Malononitrile

Triphenylamine

Photoluminescence

Electroluminescence

Electrochemistry

ABSTRACT

Three push-pull molecules with linear, quadrupolar and tripodal arrangements, consisting of triphenylamine (electro-donor) substituted with malononitrile groups (electro-acceptor), were synthesized with high yield by a simple procedure. Impact of the number of malononitrile substituents on optoelectronic properties was investigated with cyclic voltammetry, absorption and emission spectroscopy, as well as density functional theory calculation. The derivatives formed amorphous materials and exhibited low energy band gaps ranging from 2.06 to 2.49 eV. UV–Vis absorption and photoluminescence emission spectra were investigated in solutions (CHCl₃, NMP) and in solid-state as thin films and two kinds of blends (with PMMA and PVK:PBD). Quantum yield of photoluminescence was dependent on the molecule structure, solvent, and solid-state layer formulation. The compounds exhibited high photoluminescence quantum yield in the range of 15–42% and 12–59% in solid-state as film and blend with PMMA (1 wt%), respectively, being promising for applications in light emitting diodes. The diodes with active layer consisting of neat derivatives and compounds molecularly dispersed in PVK:PBD (50:50 wt%) matrix showed orange and green electroluminescence.

© 2018 Elsevier B.V. All rights reserved.

1. Introduction

Organic push-pull chromophores have become very popular being widely investigated and used as materials for optical devices as organic light-emitting diodes, organic photovoltaic cells or field effect transistors. Such a push-pull molecule exhibits D- π -A structure, i.e. donor unit, (D)- π -conjugated unit, and acceptor unit (A), where the intramolecular charge transfer can occur. Among many chemical structures having electron donor properties, triphenylamine derivatives are commonly used, while malononitrile unit is very often used as electron acceptor moieties in creation of push-pull molecules [1,2]. In the case of triphenylamine (TPA) mono-, di- and tri- substituted derivatives with malononitrile group can be synthesized having linear, quadrupolar and tripodal structures. Synthesis and some properties of substituted TPA with malononitrile groups were described in few publications. It is necessary to stress that in many papers, investigations of compounds, in which triphenylamine rings were also substituted with another

groups were presented. However, here we focus only on the results which concern triphenylamine substituted with malononitrile groups. Y. Cao et al. [3] described the dependence of fluorescence emission on various external stimuli, such as grinding, annealing and solvent fuming for triphenylamine substituted with one malononitrile group. They found that photoluminescence of the compound after grinding changed from 581 nm to 602 nm, which is a typical mechanochromic phenomenon. Interactions of triphenylaminomonomalonitrile molecules and crystal growth process were investigated by L. Kong et al. [4]. L. Kong et al. [5] investigated dependence of photoluminescence emission wavelength and quantum yield (using fluorescein as standard) and also fluorescence decay lifetime of triphenylamine-malonitrile and other compounds on various solvents (benzene, CH₂Cl₂, THF, DMF). They found that increasing solvent polarity caused red-shift of the emission wavelength. Z. Fuke et al. [6] described the results of study concerning the influence of solvent nature and its viscosity on fluorescence wavelength and quantum yield of series of compounds. They found that emission of triphenylamine-monomalonitrile was sensitive to the polarity of solvents and also that its emission is enhanced in solvents with high viscosity. The effect of solvent polarity on absorption and photoluminescence spectra of triphenylamine with mono-, di-

* Corresponding author at: Centre of Polymer and Carbon Materials, Polish Academy of Sciences, 34 M. Curie-Skłodowska Str., 41-819 Zabrze, Poland.

E-mail address: ewa.schab-balcerzak@us.edu.pl (E. Schab-Balcerzak).

and trimalonitrile units was reported by B. Li et al. [7] and S.-H. Kim et al. [8], because the solute-solvent interactions are crucial to understand molecular behavior as solvent effect may lead significant changes [9–11]. Moreover, the S.-H. Kim investigated electrochemical properties of prepared triphenylamine-mono- and di-malonitrile [8].

Triphenylamine being substituted with one malononitrile group was found to be a highly selective and sensitive fluorescent chemosensor for detection of CN^- , SO_3^{2-} and Fe^{3+} ions [12]. After addition of Fe^{3+} solution in water into the compound solution (in $\text{DMSO:H}_2\text{O}$) emission decreased gradually along with Fe^{3+} concentration, being absolutely quenched after addition of Fe^{3+} due to the consumption of the total amount of malononitrile compound in the complexation process. It is interesting that presence of other metal ions did not disturb this process. Decrease of emission band and quenching at proper amount of anions CN^- and SO_3^{2-} was also observed and the presence of other anions did not influence the process.

M. Klikar et al. [13], synthesized and investigated the properties of a series of push-pull compounds including mono, di and three substituted triphenylamine with malononitrile group. They studied their thermal and electrochemical properties, absorption in CH_2Cl_2 solution and also photoinduced piezooptical coefficients at a He-Ne laser probing wavelength at 1150 nm. However, photoluminescence of the compounds was not investigated. A series of compounds consisting of triphenylamine as donor and different substituents as electron accepting units were synthesized by R. Lartia et al. [14]. Investigations were carried out from the point of view for those materials being suitable for coupling to biomolecules. The main emphasis was put on their two-photon absorption properties. Among the other compounds, triphenylamine substituted with one, two or three malononitrile groups were investigated. It was found that three substituted triphenylamine belongs to the most efficient two photon absorption compound described in [14]. Additionally triphenylamine with two malononitrile group was found to be promising compound for labeling of biomolecules from the point of view of its two-photon absorption efficiency/molecular weight ratio. D. Cvejn et al. [15], synthesized and compared the properties of a series of triphenylamine being tri-substituted with various electron accepting units, among them also with malononitrile one. The authors detected their thermal properties, electrochemistry and absorption and photoluminescence in THF solution.

Triphenylamine with one malononitrile group dispersed in poly (9-vinylcarbazole) (PVK) was tested in the light emitting diode with configuration ITO/PVK + dye/Al and emission of orange light was observed [16,17].

In none of these works there is any investigation concerning photophysical properties of triphenylamines substituted with malononitrile groups measured in solid-state as blend and testing their electroluminescence ability in diodes, in which a neat compound create of active layer (ITO/PEDOT:PSS/compound/Al) and is dispersed in a binary matrix consists of PVK: 2-(4-biphenyl)-5-(4-*tert*-butylphenyl)-1,3,4-oxadiazole (PBD), (ITO/PEDOT:PSS/

PVK:PBD:compound (1, 2 and 15 wt%)/Al). Thus, the aim of the presented study was the synthesis, using a simple procedure, without complicated catalytic systems and with high yields, small molecules as prospective materials for light emitting applications. The malononitrile derivatives were selected because they are solid-state emissive organic materials due to aggregation-induced emission (AIE), in contrast to most of other compounds, whose emission is usually quenched in solid-state [2,18].

2. Experimental Section

2.1. Materials

Some of the commercially available chemicals were used without further purification. Solvents were purified by distillation using the standard methods and were purged with nitrogen before use. Column

chromatography was done on Merck silica gel. Thin layer chromatography (TLC) was carried out on silica gel (Merck TLC Silica Gel 60). Poly (3,4 (ethylenedioxy)thiophene): poly-(styrenesulfonate) (PEDOT:PSS) (0.1–1.0 S/cm) and substrates with pixilated ITO anodes were supplied by Ossila. Poly(9-vinylcarbazole) PVK ($M_n = 25,000\text{--}50,000$), 2-(4-biphenyl)-5-(4-*tert*-butylphenyl)-1,3,4-oxadiazole (PBD), poly (methyl methacrylate) (PMMA), Bu_4NPF_6 , NaOH, 4-(diphenylamino) benzaldehyde, 4,4'-diformyltriphenylamine, tris(4-formylphenyl) amine were purchased from Sigma Aldrich.

2.2. Typical Procedure for the Synthesis of Malononitrile Derivatives

All compounds were prepared according to the method described in our previously published paper [19].

Aluminum trioxide (0.8 g, 1.6 g and 2.4 g) and appropriate aldehyde (4 mmol) were placed in a glass-stoppered conical flask. Then solution of malononitrile (8 mmol, 16 mmol and 24 mmol) in methylene chloride (20 cm^3) was added. The reaction mixture was stirred until the complete disappearance of the starting material was determined by thin layer chromatography. Crude products were purified using column chromatography (SiO_2 , CH_2Cl_2).

[4-(Diphenylamino)benzylidene]propanedinitrile (MN-M)

Orange Solid. Yield: 84%. $^1\text{H NMR}$ (400 MHz, CDCl_3) δ 7.74 (d, $J = 9.0$ Hz, 2H), 7.52 (s, 1H), 7.43–7.35 (m, 4H), 7.27–7.18 (m, 6H), 6.95 (d, $J = 9.0$ Hz, 2H). $^{13}\text{C NMR}$ (100 MHz, CDCl_3) δ 157.9, 153.5, 145.1, 133.0, 130.0, 126.7, 126.2, 122.7, 118.4, 115.2, 114.1, 75.3. **FTIR** (KBr, cm^{-1}): 3062 (C–H stretching aromatic), 2220 (C \equiv N), 1591 (C–C stretching in the aromatic ring), 1190 (C–N stretching), 706 (C–N deformation). **Anal. Calcd** for ($\text{C}_{22}\text{H}_{15}\text{N}_3$) (321.37 g/mol): C, 82.22; H, 4.70; N, 13.08; Found: C, 82.42; H, 4.85; N, 12.77. DSC: I run: $T_m = 137$ °C, Lit. $T_m = 139$ °C [6]; II run: $T_g = 27$ °C. TGA: $T_{5\%} = 247$ °C, $T_{\text{max}} = 337$ °C.

Bis[4-(2,2-dicyanovinyl)phenyl]phenylamine (MN-D)

Red Solid. Yield: 72%. $^1\text{H NMR}$ (400 MHz, CDCl_3) δ 7.84 (d, $J = 8.8$ Hz, 4H), 7.63 (s, 2H), 7.48–7.41 (m, 2H), 7.38–7.32 (m, 1H), 7.18 (d, $J = 8.9$ Hz, 6H). $^{13}\text{C NMR}$ (100 MHz, CDCl_3) δ 157.8, 151.5, 144.6, 132.8, 130.7, 127.6, 126.2, 123.0, 114.4, 113.3, 79.9. **FTIR** (KBr, cm^{-1}): 3027 (C–H stretching aromatic), 2220 (C \equiv N), 1575 (C–C stretching in the aromatic ring), 1183 (C–N stretching), 696 (C–N deformation). **Anal. Calcd** for ($\text{C}_{26}\text{H}_{15}\text{N}_5$) (397.43 g/mol): C, 78.57; H, 3.80; N, 17.62; Found: C, 78.27; H, 3.64; N, 17.48. DSC: I run: $T_m = 230$ °C Lit. $T_m = 226$ °C [6]; II run: $T_g = 75$ °C, $T_c = 154$ °C, $T_m = 230$ °C. TGA: $T_{5\%} = 297$ °C, $T_{\text{max}} = 298,405$ °C.

Tris[4-(2,2-dicyanovinyl)phenyl]amine (MN-T)

Orange Solid. Yield: 67%. $^1\text{H NMR}$ (400 MHz, CDCl_3) δ 7.92 (d, $J = 8.8$ Hz, 6H), 7.69 (s, 3H), 7.25 (d, $J = 8.7$ Hz, 6H). $^{13}\text{C NMR}$ (100 MHz, CDCl_3) δ 157.5, 150.0, 132.8, 127.7, 124.9, 113.8, 112.8, 81.7. **FTIR** (KBr, cm^{-1}): 3069 (C–H stretching aromatic), 2217 (C \equiv N), 1571 (C–C stretching in the aromatic ring), 1193 (C–N stretching), 705 (C–N deformation). **Anal. Calcd** for ($\text{C}_{30}\text{H}_{15}\text{N}_7$) (473.48 g/mol): C, 76.10; H, 3.19; N, 20.71; Found: C, 75.74; H, 3.47; N, 20.60. DSC: I run: $T_m = 155$ °C; II run: $T_g = 99$ °C. TGA: $T_{5\%} = 271$ °C, $T_{\text{max}} = 337$ °C.

2.3. Blends and Films Preparation

Films and blends on glass substrates were prepared from a homogeneous chloroform solution (10 mg/ml) of malononitrile derivatives with PVK:PBD (50:50 in weight %) (1, 2 or 15 wt% content) and PMMA (1 wt% compound content). Films and blends with PVK:PBD were performed by spin-coating method (1000 rpm, 60 s) and blends

with PMMA by casting technique. Then films and blends were dried for 24 h in a vacuum oven at 50 °C.

2.4. OLED Preparation and Electroluminescence Measurements

Devices with sandwich configuration ITO/PEDOT:PSS/**compound**/Al and ITO/PEDOT:PSS/**compound**:PVK:PBD/Al with 1, 2 and 15 wt% of malononitrile derivatives content in blend were prepared. Devices were prepared on OSSILA substrates with pixilated ITO anodes, cleaned with detergent, deionized water, 10% NaOH solution, water and isopropyl alcohol in an ultrasonic bath. Substrates were covered with PEDOT:PSS film by spin coating at 5000 rpm for 60s and annealed for 5 min at 120 °C. Active layer was spin-coated on top of the PEDOT:PSS layer from chloroform solution (10 mg/cm³) at 1000 rpm for 60 s and annealed for 5 min at 100 °C. Finally Al was vacuum-deposited at a pressure of $5 \cdot 10^{-5}$ Torr. Electroluminescence (EL) spectra were measured with the voltage applied using a precise voltage supply (GwInstek PSP-405) and the sample was fixed to an XYZ stage. Light from the OLED device was collected through a 30 mm lens, focused on the entrance slit (50 µm) of a monochromator (Shamrock SR-303i) and detected using a CCD detector (AndoriDus 12,305). Typical acquisition times were equal to 10 s. The pre-alignment of the setup was done using a 405 nm laser. All spectra were corrected with respect to the spectral dependence of quantum efficiency of the CCD detector.

2.5. Characterization Methods

Nuclear magnetic resonance (¹H and ¹³C NMR) spectra were recorded on a Bruker AC400 spectrometer in DMSO *d*₆ as solvent and TMS as the internal standard. Infrared spectra (FTIR) were recorded on a Thermo Scientific Nicolet iS5 FT-IR Spectrometer in the range of 4000–400 cm⁻¹ as KBr pressed pellets (KBr before use was dried). Elemental analysis was performed using Vario EL III apparatus (Elementar, Germany). Differential Scanning Calorimetry (DSC) was performed using a Du Pont 1090B apparatus with a heating/cooling rate of 20 °C·min⁻¹ under nitrogen and using aluminum sample pans in the range of 0–250 °C. The glass transition temperature was recorded in the second scan after cooling. Thermogravimetric analysis (TGA) was done with a Mettler Toledo TGA STARe system with a heating rate of 10 °C·min⁻¹ in a constant stream of nitrogen (20 ml·min⁻¹) and temperature range from 50 °C to 800 °C. UV–Vis absorption spectra were performed using an Evolution 220 UV–Visible Spectrophotometer at the concentration of 10⁻⁵ mol/dm³ and 1 cm quartz cell and Jasco V-550 Spectrophotometer for films and blends. Photoluminescence spectra (PL) in solutions were performed by using Varian Carry Eclipse Spectrometer and using Hitachi F-2500 Spectrometer for blends and films PL measurements. Quantum yields (Φ_f) measurements were performed by using the integrating sphere Avantes AvaSphere-80 (Edinburgh Instruments) and absolute method. The lifetime (τ) of photoluminescence was measured with a time correlated single photon counting (TCSPC). The time-resolve measurements were performed using the picosecond pulsed diode laser, EPL-405 nm and using a 60 W microsecond Xe flash lamp. Pulse period for all measurements was equal 50 ns and PMT (Hamamatsu, R928P) as a detector. The fluorescence decay analysis was receive an instrument response function (IRF) using ludox solution and results were presented as average values of decay after exponential fitting. Electrochemical measurements (CV) were performed with Eco Chemie Autolab PGSTAT128n potentiostat. Glassy carbon (diam. 2.0 mm) served as working electrode, while platinum coil and silver wire were used as auxiliary and reference electrode respectively. All potentials were referenced with respect to the stable internal standard, which was ferrocene couple (Fc/Fc⁺). Electrochemical measurements were performed in a one-compartment cell, in CH₂Cl₂ (ACROSS Organics, 99.9% for biochemistry grade), under argon purging, with 0.2 M Bu₄NPF₆ (Aldrich, 99%) used as the supporting electrolyte salt. Each experiment was performed in air-conditioned room in

stable temperature (*t* = 20 °C). The measurements were recorded with moderate scan rate equal to 0.100 V/s. The concentration of compounds was equal 1.0 · 10⁻⁶ mol/dm³. Deaeration of the solution was assured by argon bubbling through the solution for about 10 min before every measurement.

2.6. Crystallography

The crystals of **MN-M** and **MN-D** were mounted in turn on a Gemini Ultra Oxford Diffraction automatic diffractometer equipped with a CCD detector. X-ray intensity data were collected with graphite monochromated MoK_α radiation (λ = 0.71073 Å) at 295(2) K, in the ω scan mode. Details concerning crystal data and refinement are gathered in Table 1. Lorentz, polarization and empirical absorption correction using spherical harmonics implemented in SCALE3 ABSPACK scaling algorithm [20] were applied. The structure was solved by the direct method and subsequently completed by the difference Fourier recycling. All the non hydrogen atoms were refined anisotropically using the full-matrix, least-squares technique. The Olex2 [21] and SHELXS, SHELXL [22] programs were used for all the calculations. Atomic scattering factors were incorporated in the computer programs.

3. Result and Discussion

3.1. Synthesis and Characterization

The designed malononitrile derivatives with triphenylamine structure (**MNs**) were synthesized with high yield by a simple procedure using one step Knoevenagel reaction of 4-(diphenylamino)benzaldehyde, 4,4'-diformyltriphenylamine, tris(4-formylphenyl)amine with dicyanomethane. In this condensation reaction, a dehydrating agent (aluminum oxide) was used. They form push-pull small molecules with the donor (D)-π-acceptor (A) structure (cf. Fig. 1).

The chemical structure of the synthesized compounds was confirmed by typical techniques including ¹H NMR, ¹³C NMR, FTIR and elemental analysis. The signals of protons in dicyanovinyl units in the molecules were observed as singlets in the range of 7.69–7.52 ppm (cf. Supplementary Material, Fig. S1, S3 and S4). The signals in the range of 157.89–157.47 ppm in ¹³C NMR spectra confirmed the presence of carbon atoms bonded to hydrogen in vinyl units, while the signals in the range of 113.78–115.22 ppm were due to the carbon atom in -C ≡ N groups. Signals in the range of 75.29–81.70 ppm confirmed the presence of carbon atom bounded to cyano group in the vinyl unit (cf. Supplementary Material, Fig. S2, S4 and S6). There no signals from the aldehyde group seen in target compounds. The absorption of -C ≡ N groups in the FTIR spectra was detected at 2220 cm⁻¹ for **MN-M** and **MN-D**, while the absorption band at 2217 cm⁻¹ was found for **MN-T**. The elemental analysis results confirmed the chemical structures and purity of the synthesized compounds.

Compounds were received as an orange (**MN-1** and **MN-3**) and a red (**MN-2**) solids easily soluble in polar and non-polar solvents (e.g. dimethylsulfoxide (DMSO), *N*-methyl-2-pyrrolidone (NMP), methylene chloride (CH₂Cl₂), chloroform (CHCl₃)).

3.2. Crystal and Molecular Structures

To gain insight into the molecular organization of the triphenylamine malononitrile derivatives architecture, single crystals of **MN-M** and **MN-D** were analyzed at room temperature. The crystal were obtained by slow evaporation of the acetone:methanol (1:2) solutions of the compounds. Unfortunately it has failed to obtain well-formed **MN-T** crystals. X-ray crystallography analysis indicated that **MN-M** and **MN-D** molecules existed in the monoclinic *P*2₁/*c* and orthorhombic *P*bcn space groups respectively. Crystal data and processing parameters for the compounds are given in Table 1 while ORTEP views

Table 1
Crystal data and structure refinement details of **MN-M** and **MN-D** compounds.

	MN-M	MN-D
Empirical formula	C ₂₂ H ₁₅ N ₃	C ₂₆ H ₁₅ N ₅
Formula weight	321.37	397.43
Temperature [K]	295(2)	295(2)
Crystal system	monoclinic	orthorhombic
Space group	P2 ₁ /c	Pbcn
Unit cell dimensions		
a [Å]	7.0132(3)	15.8829(7)
b [Å]	15.9088(6)	7.4025(6)
c [Å]	16.1060(6)	36.853(3)
α	90	90
β	95.218(4)	90
γ	90	90
Volume [Å ³]	1789.53(12)	4333.0(5)
Z	4	8
Calculated density [Mg/m ³]	1.193	1.218
Absorption coefficient [mm ⁻¹]	0.072	0.075
F(000)	672	1648
Crystal dimensions [mm]	0.24 × 0.17 × 0.11	0.25 × 0.15 × 0.04
θ range for data collection [°]	3.330 to 29.431	3.317 to 29.358
Index ranges	−9 ≤ h ≤ 9 −16 ≤ k ≤ 21 −22 ≤ l ≤ 16	−21 ≤ h ≤ 16 −10 ≤ k ≤ 7 −50 ≤ l ≤ 36
Reflections collected	8957	16,066
Independent reflections	4217 [R _(int) = 0.0217]	5262 [R _(int) = 0.0356]
Data/restraints/parameters	4217/0/226	5262/0/280
Goodness-of-fit on F ²	1.022	1.026
Final R indices [I > 2σ(I)]	R ₁ = 0.0470 wR ₂ = 0.1019	R ₁ = 0.0660 wR ₂ = 0.1542
R indices (all data) ^a	R ₁ = 0.0803 wR ₂ = 0.1206	R ₁ = 0.1187 wR ₂ = 0.1819
Largest diff. peak and hole	0.128 and −0.174	0.408 and −0.304
CCDC number	1,821,956	1,822,695

$$^a R_1 = \sum ||F_o| - |F_c|| / \sum |F_c|; wR_2 = (\sum |w(F_o^2 - F_c^2)|^2 / \sum (wF_o^2)^2)^{1/2}.$$

and packing diagrams are presented on the Figs. S7 and S8. The structure of **MN-M** compound is known and determined in this work is similar to that reported in Ref. [22]. The main difference was in torsion of the phenyl ring. The dihedral angles between the three phenyl rings in Li et al work [23] were 70.05(1)°, 72.667(3)° and 74.16(3)°, respectively while in this work they were 68.28(18)°, 70.05(19)°, 70.89(18)°. The difference in the morphology of a crystal was dependent on the crystallization solvent. In the cited work crystals were obtained from hexane while there was used acetone/methanol mixture. The difference in polarity of the used to crystallization solutions are responsible for changes in the molecules geometry in crystals.

In both cases the π···π and CN...π-ring stacking interactions formed dimers that was further linked to a 1D structure by H-bonding between

ciano nitrogen and phenyl hydrogen in the crystal lattice. In the **MN-M** crystal the molecules are packed in antiparallel patterns and in **MN-D** the molecules are twisted by 90° (cf. Supplementary Material, Fig. S9). The parameters of the hydrogen bonds and stacking interactions were collected in Tables S1 and S2 in Supplementary Material. The intermolecular interactions are analyzed by means of the Hirshfeld surfaces and of the corresponding 2D fingerprint plots [24–26].

The fingerprint plots and the histogram of the relative contributions to the Hirshfeld surface for the major intermolecular contacts are presented on the Fig. 2. From the histogram immediately can be seen a larger share of the C—H...N contacts (hydrogen bonds) in dicyano **MN-D** derivative than in **MN-M**. The C...C and C...H close contacts are attributed to π...π and C—H...π stacking interactions, respectively and in both cases the share of the interactions in total Hirshfeld surface area is similar (32.2% in **MN-M** and 30% in **MN-D**). Although in the case of **MN-D** the stacking interactions are stronger as indicated by the geometric parameters collected in Supplementary Material Table S2. The N...C interaction corresponds with C≡N...π contact and their participation in Hirshfeld surface area in the case of **MN-D** is much higher than in monosubstituted **MN-M**. The stronger intermolecular interactions in dicyano derivative can help to rigidify the conformations of the molecules, thereby yielding enhanced emissions. On the other hand the twisted stacking architecture of **MN-D** could result in shorter effective conjugation lengths and blue shift emission, while the planar conformation (**MN-M**) could result in increased effective lengths and red shift emission (vide infra, cf. Table 4 emission maxima in film).

3.3. Thermal Properties

Thermogravimetric analysis (TGA) and differential scanning calorimetry (DSC) were applied to estimate the thermal behavior of the prepared compounds. Thermogravimetric analysis carried out in nitrogen atmosphere showed that the obtained compounds in dependence on their structures, started decomposition at 247 (**MN-M**), 297 (**MN-D**) and 271 °C (**MN-T**), detected as temperature of 5% weight loss (T₅). All the compounds gave similar DSC thermograms and during first heating run (20 °C/min) endothermic peak confirming their melting point (T_m) was found at 137 °C, 230 °C and 155 °C for **MN-M**, **MN-D** and **MN-T**, respectively. Thus, **MNs** were obtained as crystalline compounds after synthesis. However, they could form also amorphous materials. Under the second heating scan after cooling (15 °C/min) only glass transition temperature (T_g) was seen for **MN-M** and **MN-T** at 27 and 99 °C, respectively. DSC thermogram of the disubstituted triphenylamine (**MN-D**) during the second heating run showed glass transition temperature at 75 °C, then exotherme at 154 °C due to cold crystallization (T_c) and melting endotherm at 230 °C. Thus the investigated malononitrile derivatives exhibited typical behavior for molecular

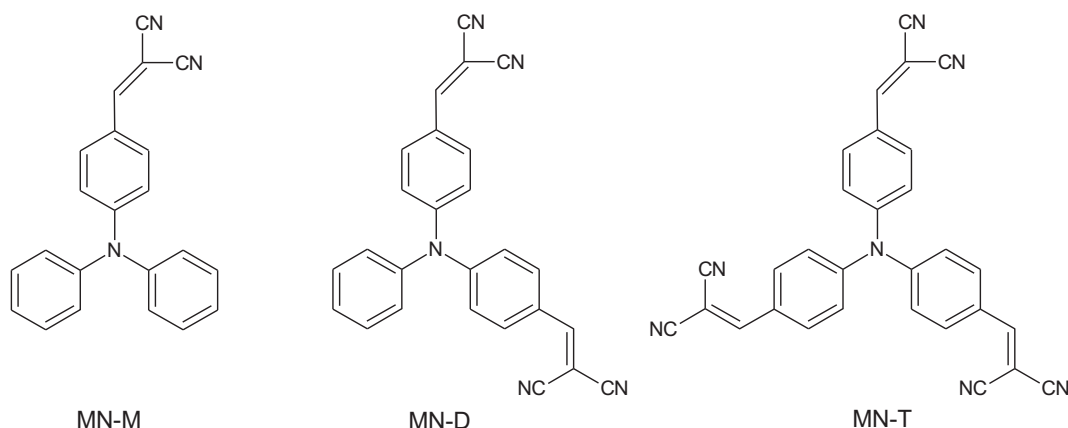


Fig. 1. Chemical structures of the investigated malononitrile derivatives (**MNs**).

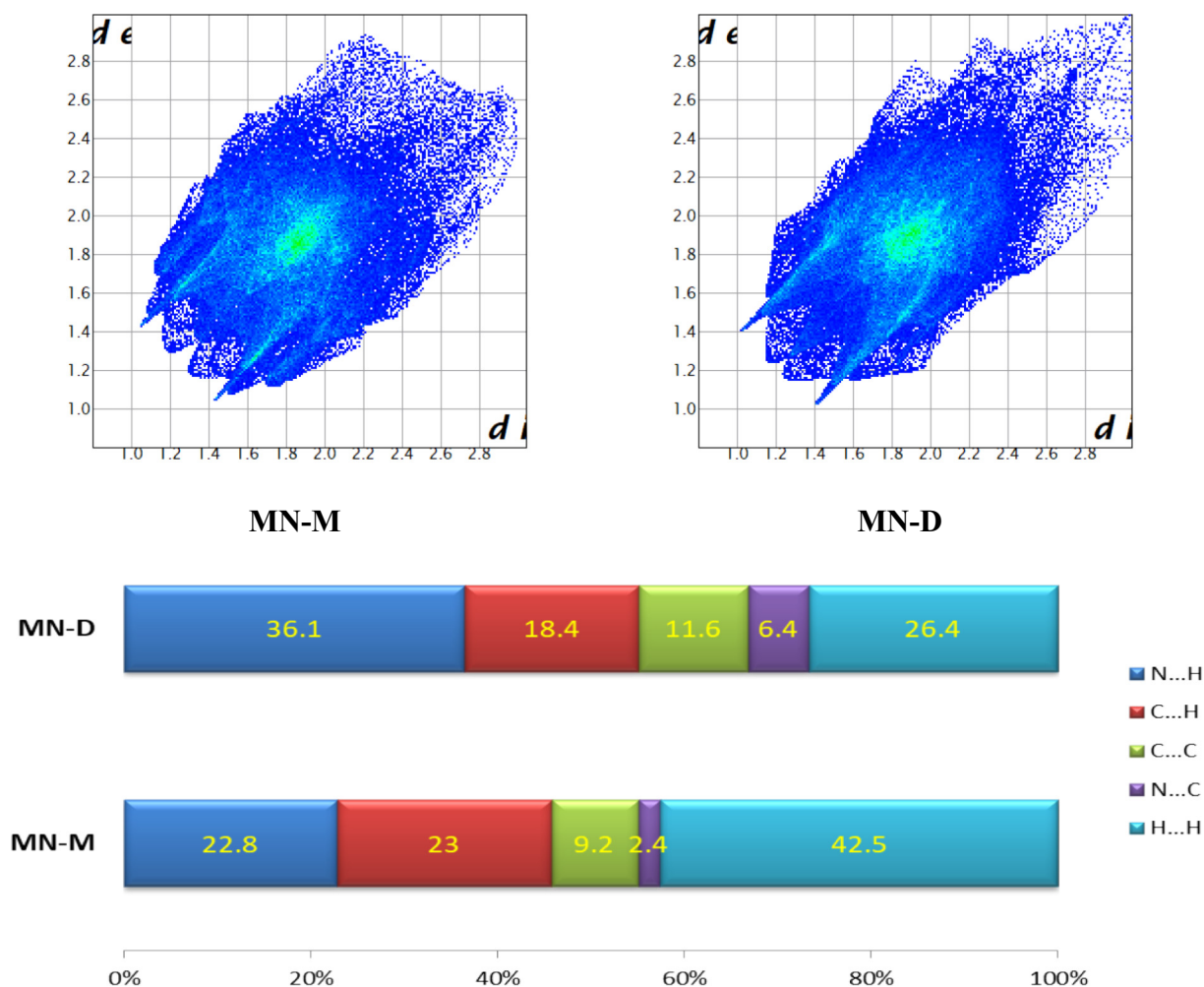


Fig. 2. Fingerprint plots and percentage contributions to the Hirshfeld surface area for the various close intermolecular contacts for **MN-M** and **MN-D** molecules.

glasses. It is interesting that **MN-D** melted at higher temperature and also exhibited higher T_5 than **MN-M** and **MN-T** (cf. Supplementary Material, Fig. S10).

3.4. DFT Calculations

The quantum theoretical calculations were used by density functional theory (DFT), with an exchange correlation hybrid functional B3LYP and the basis 6-311+G** for all atoms. The calculations were carried out with the use of Gaussian 09 program [27]. Simulated geometries of obtained compounds were optimized in vacuum. Based on the optimized geometries molecular frontier orbitals were calculated in dichloromethane. The contours of HOMOs and LUMOs are presented in Fig. 3.

The HOMO orbitals were situated on the whole molecules in the case of all compounds. As we can see, the number of malononitrile groups do not affect the location of these orbitals. On the other hand, if we take account of HOMO's values we see that amount of malononitrile groups lowers values of these orbitals (−5.79 eV for **MN-M**, −6.01 eV for **MN-D** and −6.16 eV for **MN-T**). LUMO orbitals for **MN-M** are placed only on one phenyl ring with malononitrile group. In the case of **MN-D** and **MN-T** are situated on two phenyl rings and two malononitrile groups. Interestingly, for the compound **MN-T** the LUMO orbital doesn't occur on all three phenyl ring with malononitrile groups, what could be expected. Increasing the number of -CN groups from two to three does not change the location of this orbital. Moreover, similar LUMO's values for **MN-D** and **MN-T** confirm it (−3.23 eV and −3.32 eV, cf. Table 2).

The reported molecular orbital calculations on DFT differ from presented herein HOMO, LUMO and consequently E_g value [8]. However, the same trend in HOMO's and LUMO's values was described in mentioned work

(−4.86 and −2.92 eV for **MN-M**, −5.37 and −3.57 eV for **MN-D** and −5.72 and −3.32 eV for **MN-T**).

3.5. Electrochemical Investigations

The electrochemical behavior of the triphenylamino-malonitriles was investigated using cyclic voltammetry (CV) in CH_2Cl_2 solution with glassy carbon electrode as the working electrode. The cyclic voltammograms for **MNs** are presented in Fig. 4. The electrochemical oxidation and reduction onset potentials were applied for estimation of the ionization potentials (IP) and electron affinities (EA) of the materials (assuming that IP of ferrocene equals −5.1 eV) [28]. The electrochemical data together with DFT calculated HOMO, LUMO and band gap (E_g) are presented in Table 2.

The first reduction process (E_{red}) (between −1.42 and −1.34 V) of malononitrile derivatives was irreversible ($\Delta E \geq 100$ mV). The reduction process is situated on strongly electron deficient 2,2-dicyanovinyl ($-\text{CH}=\text{C}(\text{CN})_2$) moieties [13,29]. The number of cyano groups weakly affects the first reduction onset potentials ($E_{\text{red}(\text{onset})}$), however a significant differences were seen in the case of oxidation process of **MN-M** and **MN-D** (cf. Table 2). Similar values of E_{red} for mono (**MN-M**) and di

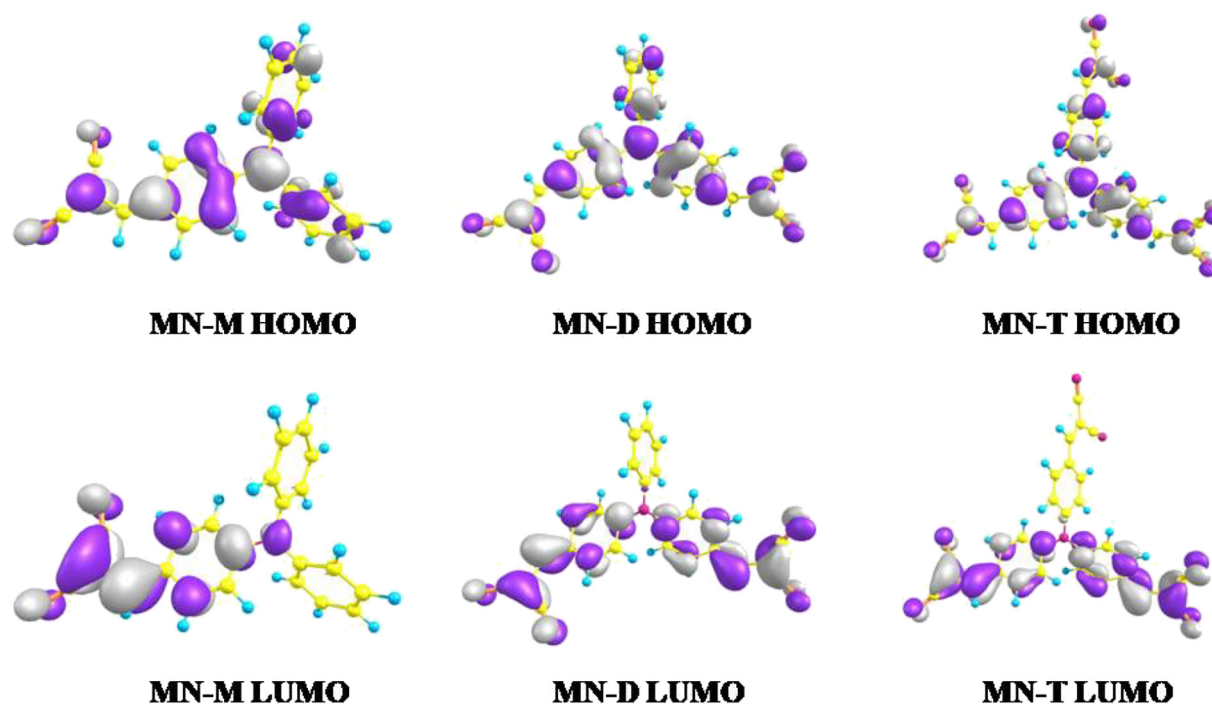


Fig. 3. HOMO, LUMO contours of the studied MNs.

(**MN-D**) substituted triphenylamine were seen. The electron affinities difference between attached one (**MN-M**), two (**MN-D**) and three (**MN-T**) malononitrile groups suggest similar acceptor strength for all malononitrile derivatives. The anodic shift of E_{red} with the increasing of acceptors was more expected [13,30].

The oxidation process is predominantly on the triphenylamine donor, nevertheless the 2,2-dicyanovinyl moieties influence was seen. The first oxidation potential for **MN-M** ($E_{\text{ox}} = 0.94$ V) is quite similar to oxidized unsubstituted triphenylamine ($E_{\text{ox}} = 0.98$ V) [31]. The E_{ox} of **MN-D** and **MN-T** in cyclic voltammetry (CV) showed the same potential peak position shifted to higher potential compare to **MN-M** (cf. Table 2). The stronger electron-donating ability of the triphenylamine donor was seen in the case of **MN-M**, as expected. S.H. Kim et al. also carried out electrochemical measurements of malononitrile substituted triphenylamines [8]. Despite the fact that, they performed the CV investigations in different experimental conditions and used a value of -4.8 as attributed to the Fc/Fc^+ couple for calculation of EA and IP, the differences compare to ours results are significant. Markedly, lower E_{g} value of malononitrile derivatives (1.49 for **MN-M** and 1.67 eV for **MN-D**) was reported [8].

Table 2
Redox potentials (vs Fc/Fc^+), IP and EA together with HOMO and LUMO and the energy band gaps of MNs.

Code	$E_{\text{ox onset}}$ (CV)	$E_{\text{red onset}}$ (CV)	IP ^a (CV)	EA ^b (CV)	HOMO ^c (DFT)	LUMO ^c (DFT)	E_{g}^{d} (DFT)	E_{g}^{e} (CV)
	[V]	[V]	[eV]	[eV]	[eV]	[eV]	[eV]	[eV]
MN-M	0.85	-1.21	-5.95	-3.89	-5.79	-2.8	2.99	2.06
MN-D	1.22	-1.23	-6.32	-3.87	-6.01	-3.23	2.78	2.45
MN-T	1.21	-1.28	-6.31	-3.82	-6.16	-3.32	2.84	2.49

^a IP = $-5.1 - E_{\text{ox onset}}$.

^b EA = $-5.1 - E_{\text{red onset}}$.

^c B3LYP/6-31++G** (d,p).

^d $E_{\text{g}} = \text{LUMO} - \text{HOMO}$.

^e $E_{\text{g}} = E_{\text{ox onset}} - E_{\text{red onset}}$.

3.6. Photophysical Properties

The optical properties of malononitrile derivatives were studied by absorption and photoluminescence (PL) spectroscopy. UV-Vis absorption and emission properties were investigated both in solutions (CHCl_3 and NMP) and in solid-state as thin film and two kinds of blend, that is, one with poly(methylmethacrylate) (PMMA) and the other with a mixture of poly(9-vinylcarbazole) (PVK) (50 wt%) and (2-(4-*tert*-butylphenyl)-5-(4-biphenyl)-1,3,4-oxadiazole) (PBD) (50 wt%). The binary blends contained 1, 2 and 15 wt% of the compounds, while PMMA contained 1 wt% of compounds. The electronic absorption data are collected in Table 3, while UV-Vis spectra in solutions are presented in Fig. 5.

UV-Vis absorption spectra of the compounds in CHCl_3 (cf. Fig. 5a) and NMP consist of two bands, one below 305 nm and the other at longer wavelengths that depended on the compounds structure and solvent polarity. Maximum absorption bands (λ_{max}) at lower wavelengths can be attributed to $\pi \rightarrow \pi^*$ transition in triphenylamine structure and λ_{max} above 350 nm to intermolecular charge transfer (ICT) [31]. Taking into consideration the solvent polarity it can be seen that maxima band absorption at longer wavelengths in less polar chloroform solution were bathochromically shifted in comparison with the ones in NMP, and the shift ranged from 65 to 123 nm depending on the compound structure. The largest shift was observed for the triphenylamine substituted with two malononitrile groups (**MN-D**) (cf. Table 3, Fig. 5a). It is interesting that in chloroform solution absorption bands of mono (**MN-M**) and tri (**MN-T**) substituted triphenylamine were found at the same wavelength $\lambda_{\text{max}} = 444$ nm, while for the disubstituted compound (**MN-D**) absorption was red shifted to $\lambda_{\text{max}} = 477$ nm. The red shift of disubstituted triphenylamine compare to mono and tri MN was also reported [13]. It is worth pointing out that the molecular absorption coefficient (ϵ) for the maximum bands is much lower (except for the second band of **MN-T**) for the compounds in NMP solution in comparison with the values in CHCl_3 solution. The effect of solvent polarity on UV-vis spectra of investigated compounds was reported by B. Li et al. [7], but not in

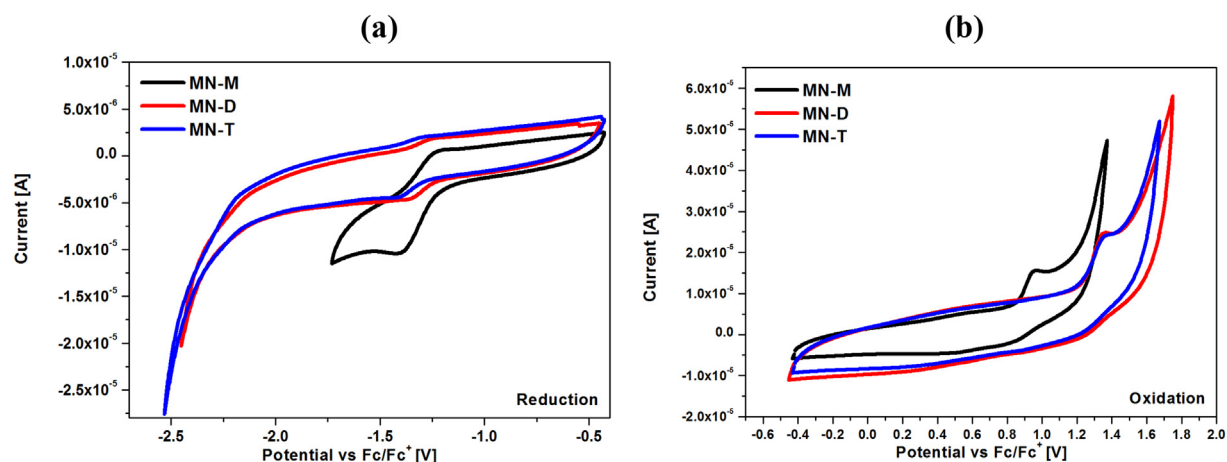


Fig. 4. Cyclic voltammograms (CV) during (a) reduction and (b) oxidation process (GC as working electrode; scan rate $0.100 \text{ V} \cdot \text{s}^{-1}$; $0.2 \text{ M Bu}_4\text{NPF}_6$ in CH_2Cl_2).

CHCl_3 and NMP and the opposite tendency, that is, positive solvatochromism was observed. S.H. Kim et al. [8] presented UV–vis spectra of MNs also in chloroform solution. However, considering the λ_{max} position of MN-M seen in its absorption spectrum at about 570 nm is significant different compare to our result [8].

The observed spectral shifts in solvents with different polarities mainly depends on the strength of the intermolecular hydrogen bonds between the substituent groups of the spectrally active molecule and the solvent molecules and whether the intramolecular hydrogen bonds are present or not. In the case of the MNs compounds no intramolecular hydrogen bonds occur and therefore the spectral shifts are sensitive to the solvent polarity. In many molecules the π - π^* bands are shifted bathochromically when the solvent polarity increases. In the case of the substituted triphenylamine compounds the hypsochromic shift in solutions is observed which suggest that the formation of H-aggregates plays an important role. The presence of aggregates is expected to diminish as the concentration of the solution is decreased and the spectra recorded in films are usually used to obtain electronic spectra from the isolated molecules. Thus the comparison of the absorption maxima of solutions and film also indicates the role of aggregates. The stronger shift in NMP suggests increase in the order within H-aggregate in more polar solvent. This conjecture is confirmed by the analysis of packing and molecular interactions in the solid-state according to which in the case of MN-D there are stronger stacking and H-bond interactions than in MN-M.

Electronic spectra were also detected for films of the compounds and their blends with PMMA and PVK:PBD. Maxima absorption bands in the films were slightly bathochromic shifted in comparison with the ones

detected in CHCl_3 solution (cf. Table 3, Fig. 5). However, it is necessary to stress that the spectrum of the disubstituted triphenylamine (MN-D) film is broader and unsymmetrical in comparison with the spectra of MN-M and MN-T films. Absorption maxima of the MNs molecularly dispersed in PMMA were hypsochromically shifted in comparison with the λ_{max} detected for their films and chloroform solution. UV–Vis spectra of the disubstituted triphenylamine (MN-D) in PMMA exhibited two separated absorption bands similarly to the spectrum of its film, however in the last case they were overlapped. In UV–vis spectra of compounds in a binary matrix absorption originating from PVK:PBD was also seen at 300 nm.

The studied derivatives exhibited significantly higher photoluminescence in CHCl_3 than in more polar solvent, that is, NMP. In Fig. 6 emission spectra and pictures taken under UV irradiation ($\lambda_{\text{ex}} = 366 \text{ nm}$) of MNs are presented, whereas the PL spectroscopic data are collected in Table 3.

In all the cases only one emission band was detected and the PL intensity was dependent on the excitation wavelengths (λ_{ex}) in the solutions (cf. Table 4). Generally the investigated compounds in CHCl_3 solution emitted light at longer wavelengths than in NMP. MN-D and MN-T in chloroform emitted green and orange light, respectively (cf. Fig. 6a), whereas in NMP they emit blue light. It was reported that the emission spectra of MNs may showed both positive and negative solvatochromism with increasing solvent polarity [8]. It was found that the emission wavelengths of MN-M and MN-T differ very little in CHCl_3 , while the emission band of MN-D is blue shifted in comparison with the MN-M and MN-T. The PL quantum yield (Φ_{PL}) in chloroform was found to be in the range of 11.9–32.4%, with the highest result for

Table 3
The electronic absorption data of malononitrile derivatives.

Code	UV–Vis λ_{max} [nm] ($\epsilon \cdot 10^4$) ^a						
	CHCl_3 ^b $\epsilon = 4.81$ ^c	NMP ^b $\epsilon = 33.00$ ^c	Film	Blend PMMA 1 wt%	Blend PVK:PBD 1 wt%	Blend PVK:PBD 2 wt%	Blend PVK:PBD 15 wt%
MN-M	290 (3.1)	298 (1.8)	445	438	460	450	450
	444 (9.3)	379 (2.3)					
MN-D	281 (2.0)	354 (1.6)	452	393	485	485	402
	395 (2.2)		502 ^{sh}	470			485
MN-T	477 (6.3)						
	250 (9.9)	305 (3.0)	468	431	450	475	473
	444 (5.6)	340 (2.6)					

^a ϵ - Absorption coefficient, [$\text{dm}^3 \cdot \text{mol}^{-1} \cdot \text{cm}^{-1}$].

^b $c = 10^{-5} \text{ mol/dm}^3$, solvents: chloroform, N-methyl-2-pyrrolidone.

^c Dielectric constant. PVK:PBD - 50:50 wt%.

^{sh} Shoulder.

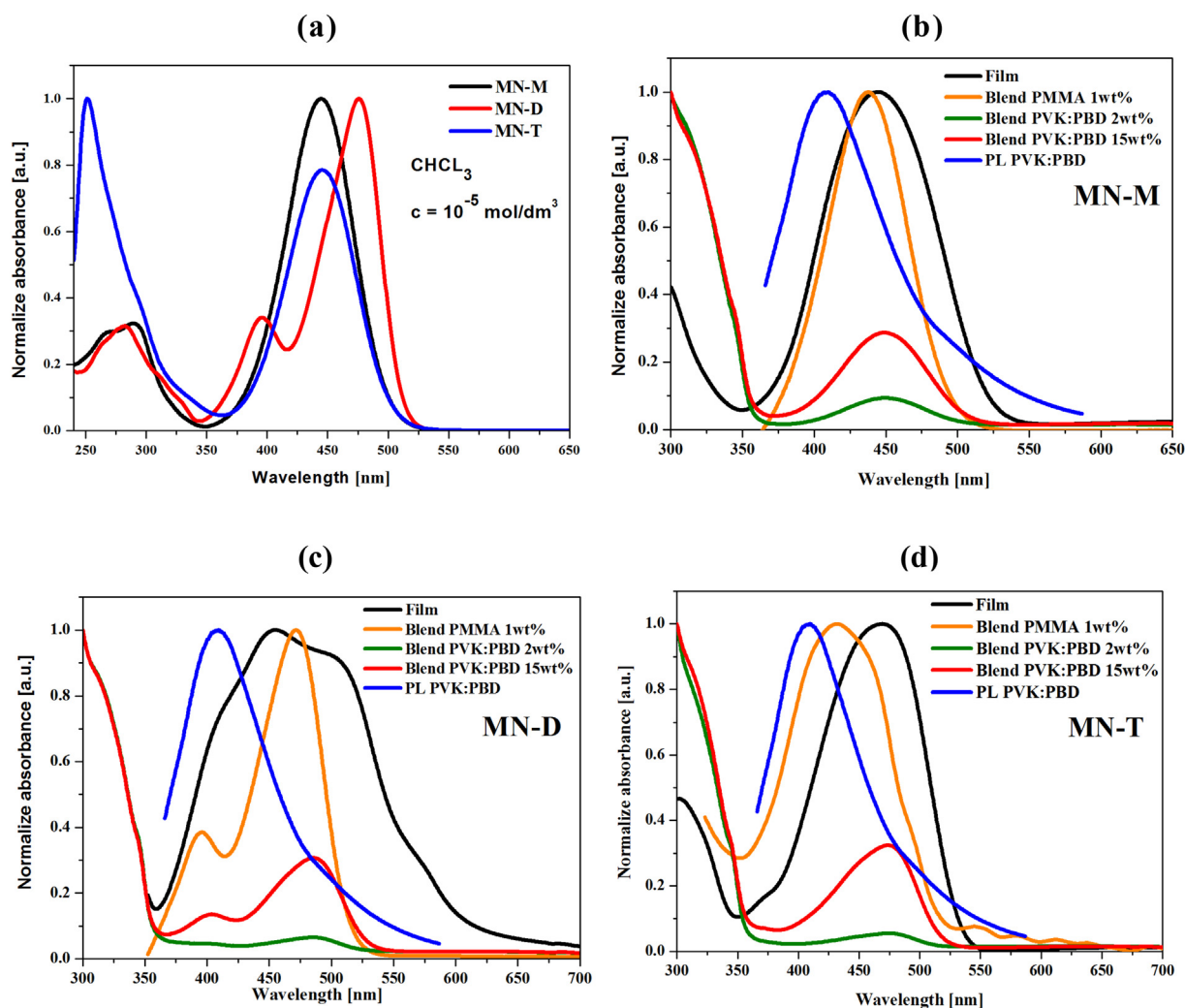


Fig. 5. UV-vis of the compounds in (a) chloroform solution and (b) – (d) in film, blend PMMA and PVK:PBD together with PL spectrum of PVK:PBD matrix ($\lambda_{\text{ex}} = 340$ nm).

trisubstituted triphenylamine (**MN-T**). This confirms that in CHCl_3 solution quantum yield increased with the number of malononitrile groups in the compound. The reported relative photoluminescence quantum yield determined using standards (quinine sulfate and/or fluorescein) in various solvents was in the range of 0.01–0.192 [7,8]. The life-time (τ_{PL}) measurements were carried out and the values of τ_{PL} were calculated, the longest decay was found for monosubstituted compound (**MN-M**) (cf. Table 4). Maxima emission bands in the films were red shifted in comparison with the ones in CHCl_3 solution for **MN-D** and **MN-T**. The longest wavelength of emitted light in film was recorded for **MN-T** (cf. Table 4).

In order to clarify the observed blue shift in the PL maxima in a polar NMP solvent, the geometries of the first singlet and triplet excited states of the compounds were optimized at the TD-B3LYP/6-311+G** level in both solvents. The calculated dipole moments in the first excited states are lower than in ground state (cf. Supplementary Material, Table S3) therefore in less polar solvent (CHCl_3 vs NMP) the stabilization of the excited state are expected. Moreover the emission originates from LUMO→HOMO transition and the energy difference between these levels is lower in chloroform than in NMP (cf. Supplementary Material, Fig. S11). The maximum difference between S1 energy gaps in chloroform and NMP was calculated for **MN-D** compound, that is for the one for which the greatest solvent effect is observed. Therefore, it can be concluded that the blue shift of absorption and emission bands in chloroform compared with NMP is caused, on the one hand, by formation of

H-aggregates in solutions, and on the other by a lower dipole moment of the excited state compared to the ground one, which affects its stabilization in less polar solvents.

Maxima emission bands (λ_{em}) of the compounds in blends with PMMA were hypsochromic shifted in comparison with the emission of the films and the differences were observed in the range of 63 nm (**MN-D**) to 83 nm (**MN-T**) (cf. Supplementary Material, Fig. S12, S13). In the case of films the ϕ_{PL} were higher than in solution for **MN-M** and **MN-T** and reached the values of 26.5% and 42.5%, respectively. Triphenylamine with two malononitrile units (**MN-D**) exhibited slightly lower ϕ_{PL} in film (17.7%) than in solution. The PL quantum yield of the compounds in PMMA blends increased with the increasing of the nitrile groups and was found as 12.4, 55.0 and 58.7% for **MN-M**, **MN-D** and **MN-T**, respectively. In the case of a binary matrix (PVK:PBD) the hypsochromic shift of the λ_{em} was also observed in comparison with the one detected in a neat film (cf. Fig. 6, Table 4). Increasing the compounds content in a binary blends caused the red shift of the maximum emission band originating from **MNs** (cf. Table 4, cf. Supplementary Material, Fig. S14). The opposite behavior was registered in the case of PVK:PBD with 1 and 2 wt% for **MN-T**. In the PL spectra of the most of the blends with PVK:PBD, the emission of matrix in the range of 369–413 nm was seen and it suggests not complete energy transfer from the matrix to the luminophore (cf. Fig. 6b,c,d). In the case of PVK:PBD blend with the lowest **MNs** content the emission of matrix is dominating, expect for **MN-T**. Energy transfer from host (binary matrix)

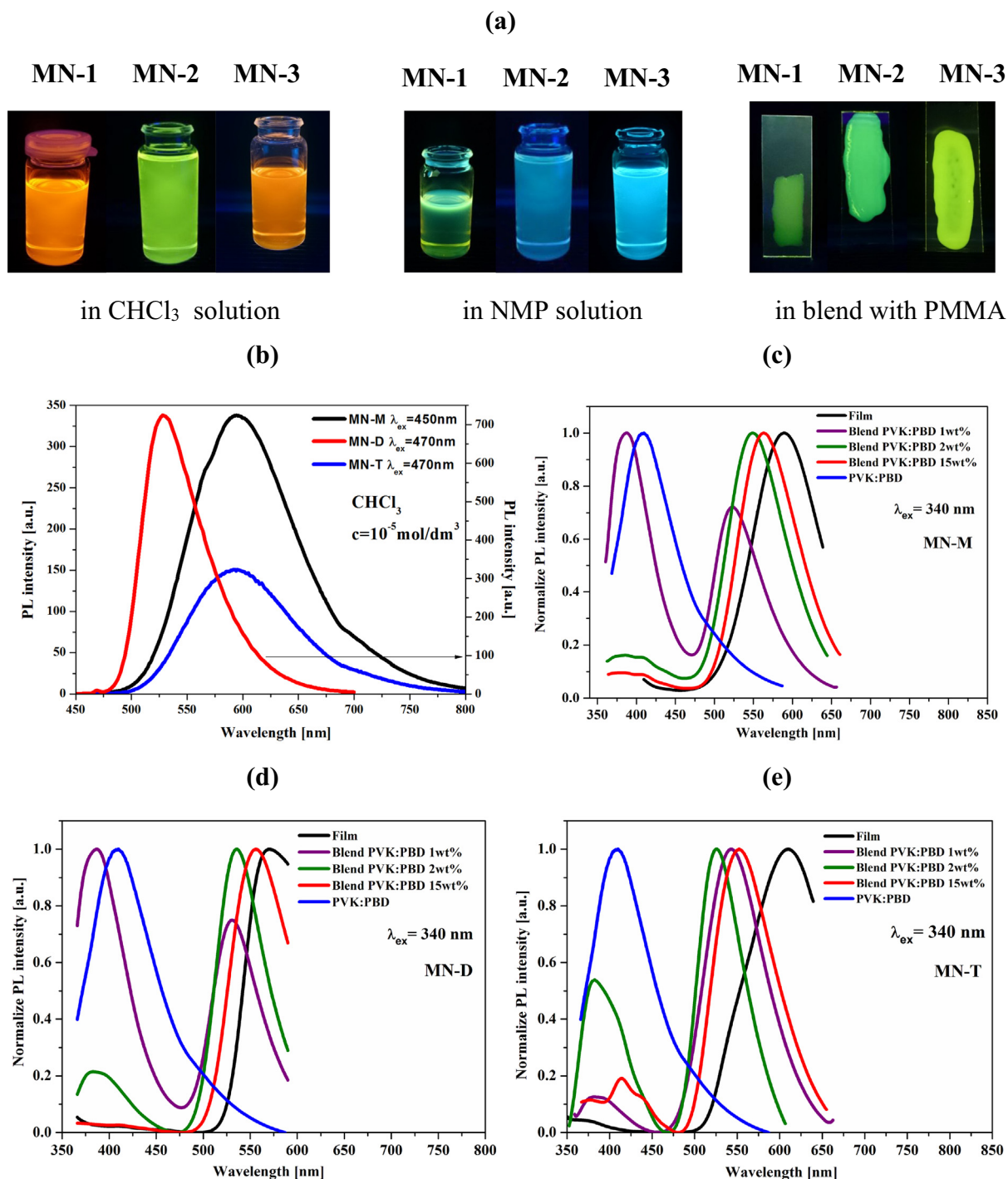


Fig. 6. (a) Photographs of investigated malononitrile derivatives under UV irradiation $\lambda_{\text{ex}} = 366$ nm, (b) - (e) PL spectra of MNs in chloroform solution and in solid-state.

to guest (chromophore) via Förster energy transfer (FRET) can take place when the PL spectrum of the host matrix overlaps with the UV-vis spectrum of the guest luminophore [32]. Energy transfer may occur as well by Dexter energy transfer, however, Dexter energy transfer requires matching the energy levels of the single and triplet excitons in the host with the energy levels of the excitons in the guest [33]. The absorption of the investigated MNs overlapped with PL of a matrix (cf. Fig. 5). The negligible PL of matrix for blend with 15 wt% of MN-D was found, which let us to conclude that the energy transfer is almost complete. The quantum yield of binary blends containing 1 wt% of the compounds increased with the malononitrile groups number and

maxima of Φ_{PL} ranged from 28.5% to 51.9%. Increase of compound content in blend affected in a different way PL quantum yield in dependence on the number of malononitrile units. It was observed that the highest Φ_{PL} was estimated for 15, 2 and 1 wt% of compound MN-M, MN-D and MN-T dispersed in a binary matrix, respectively. One can notice that the photoluminescence quantum yield of MNs in the PVK:PBD matrix for the lowest luminophore content (1 wt%) is higher than the quantum yield measured for the photoluminescence in solution (cf. Table 4). The decrease of Φ_{PL} of PVK:PBD blends together with increase of MN-D and MN-T content may indicate that in these layers there exist intermolecular interactions which quench the emission,

Table 4
Photoluminescence spectroscopic data of the malononitrile derivatives.

Code	Medium	PL				
		λ_{ex} [nm]	λ_{em} [nm]	Stokes shift [cm^{-1}] ^a	Φ [%] (τ [ns])	
MN-M	CHCl ₃ ^b	310	596	5744	–	
		340	596	5744	–	
		450	596	5744	11.9 (2.0)	
	NMP ^b	310	443	3812	–	
		340	443	3812	–	
	Film	310	591	5551	15.4	
		340	591	5551	20.1	
	Blend PMMA 1 wt% ^c	450	591	5551	26.5	
		440	516	3451	12.4	
	Blend PVK:PBD 1 wt% ^c	310	<u>385,523</u>	–	28.6	
		340	<u>385,523</u>	–	2.7;28.4	
	Blend PVK:PBD 2 wt% ^c	450	523	2619	8.8	
		310	<u>374,550</u>	–	31.4	
	Blend PVK:PBD 15 wt% ^c	340	<u>374,550</u>	–	22.9	
		450	550	4040	33.7	
	MN-D	CHCl ₃ ^b	310	369,564	–	30.1
			340	<u>385,564</u>	–	30.8
			450	564	1049	38.7
		NMP ^b	310	526	1953	–
			340	526	1953	–
		Film	400	526	1953	15.4
			470	526	1953	18.7(1.1)
		Blend PMMA 1 wt% ^c	310	574	4702	17.7
			340	574	4702	17.1
Blend PVK:PBD 1 wt% ^c		400	574	4702	13.2	
		480	574	4702	15.4	
Blend PVK:PBD 2 wt% ^c		400	511	1707	50.3	
		470	511	1707	54.9	
Blend PVK:PBD 15 wt% ^c		310	<u>385,532</u>	–	32.8	
		340	<u>385,532</u>	–	3.4;30.6	
Blend PVK:PBD 2 wt% ^c		490	532	1962	22.7	
		310	<u>383,536</u>	–	35.8	
Blend PVK:PBD 15 wt% ^c		340	<u>383,536</u>	–	2.4;34.5	
		490	536	1962	32.0	
MN-T		CHCl ₃ ^b	310	<u>371,557</u>	–	23.9
			340	557	2665	23.7
			400	557	2665	18.9
		NMP ^b	490	557	2665	25.2
			310	593	5659	–
	Film	340	593	5659	–	
		450	593	5659	21.1	
	Blend PMMA 1 wt% ^c	470	593	5659	32.4(1.9)	
		310	455	7434	–	
	Blend PVK:PBD 1 wt% ^c	340	455	7434	–	
		310	604	4811	19.6	
	Blend PVK:PBD 2 wt% ^c	340	604	4811	16.8	
		410	604	4811	42.5	
	Blend PVK:PBD 15 wt% ^c	470	604	4811	15.0	
		430	521	4008	42.7	
	Blend PMMA 1 wt% ^c	450	521	4008	58.7	
		310	<u>377,542</u>	–	51.9	
	Blend PVK:PBD 1 wt% ^c	340	<u>377,542</u>	–	51.3	
		470	542	3772	39.0	
	Blend PVK:PBD 2 wt% ^c	310	<u>381,526</u>	–	14.1	
		340	<u>381,526</u>	–	13.3	
	Blend PVK:PBD 15 wt% ^c	470	526	2041	24.0	
		310	<u>375,553</u>	–	8.0	
	Blend PVK:PBD 15 wt% ^c	340	<u>413,553</u>	–	9.1	
470		553	3058	11.5		

Bold data indicates the most intense PL. Underlined data indicates the dominant band.

^a Stokes shifts calculated according to the equation $\Delta\nu = (1/\lambda_{\text{abs}} - 1/\lambda_{\text{em}}) \cdot 10^7$ [cm^{-1}].

^b c = 10^{-5} mol/dm³.

^c wt% - concentration of compound in blend PMMA or PVK:PBD (50 wt%:50 wt%).

contrary to the behavior seen for **MN-M**. It can be concluded that the number of malononitrile units linked with triphenylamine structure significantly affects the luminescence ability of the studied compounds. The AIE phenomena seems to be weaker together with the increase of number of malononitrile groups.

3.7. Electroluminescence Study

Electroluminescence (EL) ability of the **MNs** was tested in diodes with two structure types. Diodes with configuration of ITO/PEDOT:PSS/**compound**/Al and ITO/PEDOT:PSS/PVK:PBD:**compound** (1, 2 and 15 wt%)/Al were fabricated. The EL spectra of selected diodes and HOMO (IP) and LUMO (EA) energy levels of device components are presented in Fig. 7 and in Supplementary Material (cf. Fig. S15). All prepared diodes under external voltage emitted light (cf. Table 5). We are aware, that for detailed discussion of OLED performance the luminance or power intensities of EL should be given.

However, we present in this work preliminary investigations aimed at testing only the ability of **MNs** for EL and at this stage we have experimental capability to register electroluminescence spectra only. Thus, the position of λ_{EL} and intensity of the EL emission band can be disused. The maximum emission band (λ_{EL}) in the range of 532–653 nm was observed. Diodes with configuration ITO/PEDOT:PSS/**compound**/Al emitted red (**MN-M**, **MN-T**) and orange (**MN-D**) light under external voltage in the range of 6–10 V (cf. Table 5, Fig. 7), whereas the diodes with compounds dispersed in PVK:PBD matrix emitted green light. The red shift of EL with increasing of the **MNs** content in matrix was seen except for **MN-T** with 2 wt%. It should be stressed that the highest EL intensity was found for diodes based on neat compounds. Considering the devices with such active layers the EL intensity increased in the following order **MN-T** < **MN-D** < **MN-M**. This rule also concerns the diodes with 1 wt% of **MNs** in PVK:PBD matrix. Generally, the increase of **MNs** content in active layer resulted in lowering the light intensity. Together with increase of external voltage the increase of EL intensity without changes of λ_{EL} position was seen.

4. Conclusions

Three molecules consisting of triphenylamine being functionalized with one, two and three malononitrile groups were prepared and investigated. The impact of the number of malononitrile substituents in the molecules on their selected properties was presented. These compounds can formed glassy state and together with increase of number of malononitrile units the increased of T_g from 27 °C to 99 °C was detected. They showed the similar low E_g value, slightly lower about 0.1 eV for molecule with two malononitrile units (**MN-D**). The results of CV measurements show that the ionization potential decrease with increase of number malononitrile groups from one to two in molecule. The studied **MNs** were emissive in solution and in solid-state. The polarity of the solvent significantly influenced on the absorption and photoluminescence range and negative solvatochromic effect was observed. It can be noticed that compounds with one and three malononitrile groups (**MN-M** and **MN-T**) exhibited the similar UV–vis absorption and photoluminescence range. Whereas, the absorption and emission of disubstituted triphenylamine (**MN-D**) was bathochromically and hypsochromically shifted, respectively. Together with increase on malononitrile units number more efficient PL with Φ_{PL} up to 58.7% in solution and in solid-state solid-state as film and blend with PMMA was seen (except for **MN-D** in film). Considering the PL in a binary matrix only in the case of compound with one malononitrile unit (**MN-M**) the highest its content resulted in raising of Φ_{PL} . Optimal content of **MN-D** and **MN-T** in PVK:PBD which gives the highest PL was 2 and 1 wt%. It seems that an AIE phenomenon is weaker in di- and trisubstituted triphenylamine. It was demonstrated that the compounds are electroluminescent and diode with a neat malononitrile derivatives as active layer emitted light with λ_{EL} the located at 603–653 nm. Whereas, utilization of them as component of active layer gives emission of green light by devices. To the best of our knowledge, the first time, ability for electroluminescence of triphenylamines functionalized with malononitrile groups is presented.

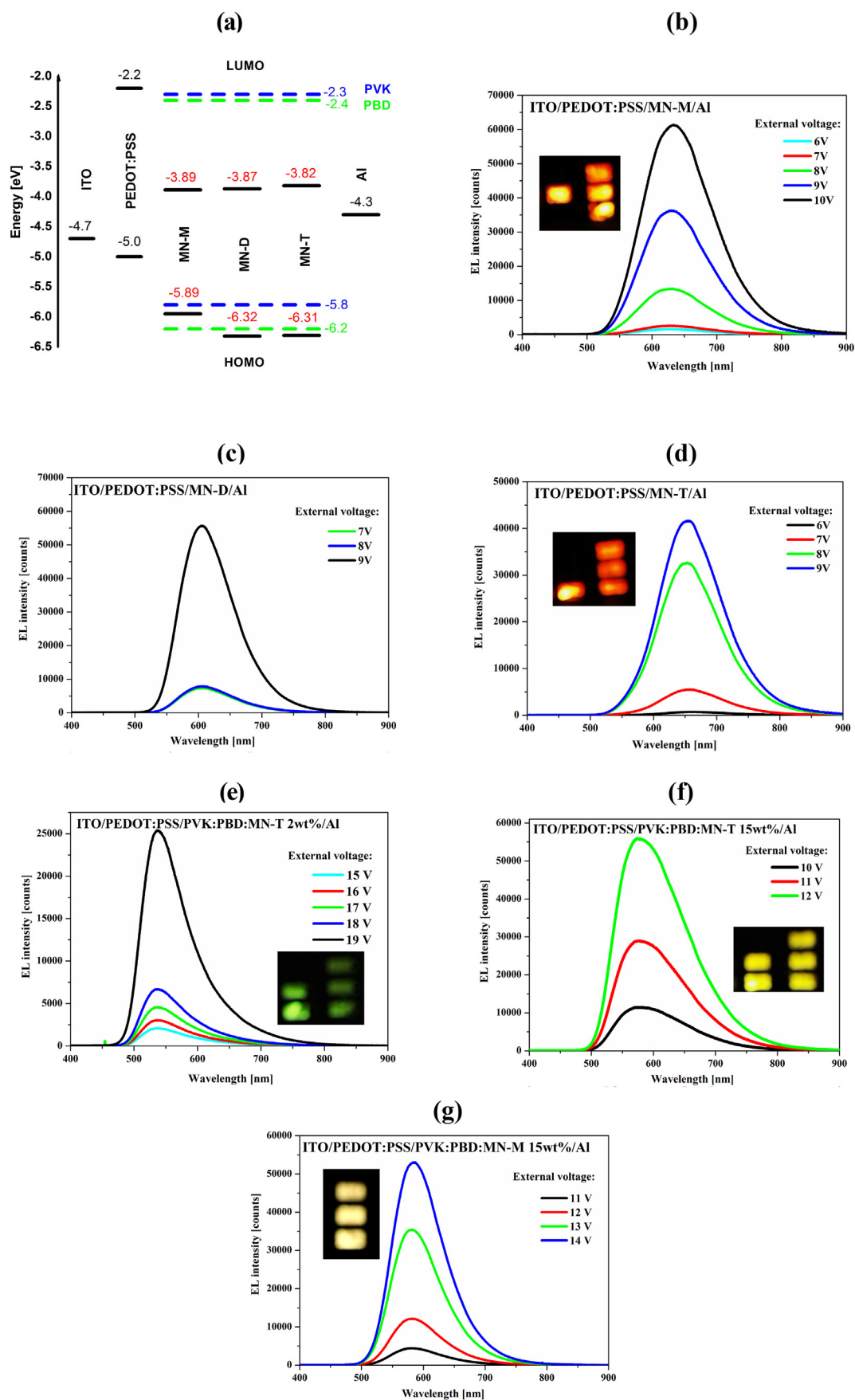


Fig. 7. (a) HOMO and LUMO energy levels of diode components and (b) - (g) electroluminescence spectra with photographs of working devices of investigated malononitrile derivatives.

Table 5
Maximum of EL band and its intensity.

Code	EL ^a	λ _{EL}	EL ^b	λ _{EL}	EL ^c	λ _{EL}	EL ^d	λ _{EL}
	intensity	[nm]	intensity	[nm]	intensity	[nm]	intensity	[nm]
	[counts]	[nm]	[counts]	[nm]	[counts]	[nm]	[counts]	[nm]
MN-M	61,290	632	58,580	532	52,660	551	53,064	584
MN-D	55,820	603	55,270	537	1856	545	25,700	553
MN-T	41,700	653	1112	559	25,520	535	56,450	573

^a ITO/PEDOT:PSS/MNs/Al.^b ITO/PEDOT:PSS/PVK:PBD:MNs 1 wt%/Al.^c ITO/PEDOT:PSS/PVK:PBD:MNs 2 wt%/Al.^d ITO/PEDOT:PSS/PVK:PBD:MNs 15 wt%/Al.

Acknowledgments

This work was supported by National Science Centre of Poland Grants: 2015/17/N/ST5/03892. Calculations have been carried out using resources provided by Wrocław Centre for Networking and Supercomputing (<http://wccs.pl>), grant No. 18. We thank dr H. Janeczek for DSC measurements and K. Bednarczyk for TGA measurements.

Appendix A. Supplementary Data

CIF files giving crystallographic data for **MN-M** and **MN-D** (CCDC 1821956, 1822695) can be obtained free of charge via www.ccdc.cam.ac.uk/data_request/cif or from the Cambridge Crystallographic Data Centre, 12 Union Road, Cambridge CB2 1EZ, UK; fax: +44 1223-336-033. Supplementary data to this article can be found online at <https://doi.org/10.1016/j.saa.2018.11.025>.

References

- Z. Ning, H. Tian, *Chem. Commun.* 37 (2009) 5483–5495.
- Z. Ning, Z. Chen, Q. Zhang, Y. Yan, S. Qian, Y. Cao, H. Tian, *Adv. Funct. Mater.* 17 (2007) 3799–3807.
- Y. Cao, W. Xi, L. Wang, h. Wang, L. Kong, H. Zhou, J. Wu, Y. Tian, *RSC Adv.* 4 (2014) 24649–24652.
- L. Kong, J.-X. Yang, L.-J. Cheng, P. Wang, H.-P. Zhou, J.-Y. Wu, Y.-P. Tian, B.-K. Jin, X.-T. Tao, *J. Mol. Struct.* 1059 (2014) 144–149.
- L. Kong, Y.J. Yang, H. Zhou, S. Li, F. Hao, Q. Zhang, Y. Tu, J. Wu, Z. Xue, Y. Tian, *Sci. China Chem.* 56 (2013) 106–116.
- F. Zhou, J. Shao, Y. Yang, J. Zhao, H. Guo, X. Li, S. Ji, Z. Zhang, *Eur. J. Org. Chem.* 25 (2011) 4773–4787.
- Y. Yang, B. Li, L. Zhang, *Sens Actuators B Chem.* 183 (2013) 46–51.
- L. Xiaochuan, S. Young-A, K. Young-Sung, K. Sung-Hoon, K. Jun, S. Jong-I, *J. Nanosci. Nanotechnol.* 12 (2012) 1497–1502.
- M. Kurban, B. Gündüz, *J. Mol. Struct.* 1137 (2017) 403–411.
- M. Kurban, B. Gündüz, *Optik* 165 (2018) 370–379.
- B. Gündüz, M. Kurban, *Vib. Spectrosc.* 96 (2018) 46–51.
- X. Yang, X. Chen, X. Lu, Ch. Yan, Y. Xu, X. Hang, J. Qu, R. Liu, *J. Mater. Chem. C* 4 (2016) 383–390.
- M. Klikar, I.V. Kityk, D. Kulwas, T. Mikysek, O. Pytela, F. Bures, *New J. Chem.* 41 (2017) 1459–1472.
- R. Lartia, C. Allain, G. Bordeau, F. Schmidt, C. Fiorini-Debuisschert, F. Charra, M.-P. Teulade-Fichou, *J. Org. Chem.* 73 (2008) 1732–1744.
- D. Cvejn, E. Michail, I. Polyzos, N. Almonasy, O. Pytela, M. Klikar, T. Mikysek, V. Giannetas, M. Fakis, F. Bures, *J. Mater. Chem. C* 3 (2015) 7345–7355.
- W. Brutting, S. Berleb, G. Egerer, M. Schwoerer, R. Wehrmann, A. Elschner, *Synth. Met.* 91 (1997) 325–327.
- S. Berleb, W. Brutting, M. Schwoerer, *J. Appl. Phys.* 83 (1998) 4403–4409.
- J. Luo, Z. Xie, J.W.Y. Lam, L. Cheng, H. Chen, C. Qiu, H.S. Kwok, X. Zhan, Y. Liu, D. Zhu, B.Z. Tang, *Chem. Commun.* (18) (2001) 1740–1741.
- A. Szłapa, S. Kula, U. Błaszkiwicz, M. Grucela, E. Schab-Balcerzak, M. Filapek, *Dyes Pigments* 129 (2016) 80–89.
- CrysAlisPro 1.171.38.46, Rigaku Oxford Diffraction 2015.
- O.V. Dolomanov, L.J. Bourhis, R.J. Gildea, J.A.K. Howard, H. Puschmann, *J. Appl. Crystallogr.* 42 (2009) 339–341.
- G.M. Sheldrick, *Acta Cryst C* 71 (2015) 3–8.
- X.C. Li, W.T. Lim, S.H. Kim, Y.A. Son, *New Cryst. Struct.* 224 (2009) 493–494.
- M.A. Spackman, D. Jayatilaka, *CrystEngComm* 11 (2009) 19–32.
- M.A. Spackman, J.J. McKinnon, *CrystEngComm* 4 (2002) 378–392.
- S.K. Wolff, D.J. Grimwood, J.J. McKinnon, M.J. Turner, D. Jayatilaka, M.A. Spackman, *CrystalExplorer* (version 3.1), University of Western Australia, 2012.
- M.J. Frisch, G.W. Trucks, H.B. Schlegel, G.E. Scuseria, M.A. Robb, J.R. Cheeseman, G. Scalmani, V. Barone, B. Mennucci, G.A. Petersson, H. Nakatsuji, M. Caricato, X. Li, H.P. Hratchian, A.F. Izmaylov, J. Bloino, G. Zheng, J.L. Sonnenberg, M. Hada, M. Ehara, K. Toyota, R. Fukuda, J. Hasegawa, M. Ishida, T. Nakajima, Y. Honda, O. Kitao, H. Nakai, T. Vreven, J.A. Montgomery Jr., J.E. Peralta, F. Ogliaro, M. Bearpark, J.J. Heyd, E. Brothers, K.N. Kudin, V.N. Staroverov, R. Kobayashi, J. Normand, K. Raghavachari, A. Rendell, J.C. Burant, S.S. Iyengar, J. Tomasi, M. Cossi, N. Rega, J.M. Millam, M. Klene, J.E. Knox, J.B. Cross, V. Bakken, C. Adamo, J. Jaramillo, R. Gomperts, R.E. Stratmann, O. Yazyev, A.J. Austin, R. Cammi, C. Pomelli, J.W. Ochterski, R.L. Martin, K. Morokuma, V.G. Zakrzewski, G.A. Voth, P. Salvador, J.J. Dannenberg, S. Dapprich, A.D. Daniels, O. Farkas, J.B. Foresman, J.V. Ortiz, J. Cioslowski, D.J. Fox, Gaussian Inc, Gaussian 09, Revision A.1, Wallingford CT, 2009.
- P. Bujak, I. Kulszewicz-Bajer, M. Zagorska, V. Maurel, I. Wielgus, A. Pron, *Chem. Soc. Rev.*, 2013,42, 8895–999.
- S. Kotowicz, S. Kula, M. Filapek, A. Szłapa-Kula, M. Siwy, H. Janeczek, J.G. Malecki, K. Smolarek, S. Maćkowski, E. Schab-Balcerzak, *Mater. Chem. Phys.* 209 (2018) 249–261.
- X. Tang, W. Liu, J. Wu, C.-S. Lee, J. You, P. Wang, *J. Org. Chem.* 75 (2010) 7273–7278.
- E.T. Seo, R.F. Nelson, J.M. Fritsch, L.S. Marcoux, D.W. Leedy, R.N. Adams, *JACS* 88 (1966) 3498–3503.
- K. Kotwica, P. Bujak, D. Wamil, A. Pieczonka, G. Wiosna-Salyga, P.A. Gunka, T. Jaroch, R. Nowakowski, B. Luszczynska, E. Witkowska, I. Glowacki, J. Ulanski, M. Zagorska, A. Pron, *J. Phys. Chem. C* 119 (2015) 1070–10708.
- J.W. Kim, S. Il You, N.H. Kim, J.-A. Yoon, K.W. Cheah, F.R. Zhu, W.Y. Kim, *Sci. Rep.* 4 (2014) 7009.